Effect of fouling and cleaning upon the surface charge and porosity of polyethersulphone membranes during coffee brew decaffeination

Manios Triantafyllos K., Pihlajamäki Arto, Mattia Davide, Bird Michael R.

DOI: 10.1016/j.fbp.2023.07.005

Available online at www.sciencedirect.com

Food and Bioproducts Processing

journal homepage: www.elsevier.com/locate/fbp

Effect of fouling and cleaning upon the surface charge and porosity of polyethersulphone membranes during coffee brew decaffeination

Triantafyllos K. Manios[a], *Arto Pihlajamäki*[b], *Davide Mattia*[a], *Michael R. Bird*[a,*]

[a] *Centre for Advanced Separations Engineering (CASE), Department of Chemical Engineering, University of Bath, BA2 7AY, UK*

[b] *LUT School of Engineering Science, LUT University, P.O. Box 20, Lappeenranta 53851, Finland*

ARTICLE INFO

Article history:
Received 27 April 2023
Received in revised form 13 July 2023
Accepted 19 July 2023
Available online 22 July 2023

Keywords:
Coffee
Decaffeination
Membranes
Fouling
Cleaning
Zeta potential

ABSTRACT

Filtration processes could offer a viable alternative to use of solvents for the production of reduced caffeine coffee beverages (so called 'half-decaf') which have recently gained increased commercial attention. However fouling phenomena and membrane deterioration could significantly alter the process performance; hence fouling and cleaning mitigation strategies must be explored by monitoring key membrane properties such as porosity and surface charge. In this study, multiple cycle filtration of coffee brews for the selective reduction of caffeine has been performed. A commercially available synthetic tight ultrafiltration polyethersulphone (PES) membrane (GP95PP – Alfa Laval) and a bespoke loose nanofiltration mixed matrix PES membrane fabricated, were used for three consecutive fouling and cleaning filtration cycles. The impact and mechanisms of fouling and the cleaning protocol effectiveness were investigated using surface charge, porosity, membrane surface and membrane morphology characterization techniques. Streaming potential studies revealed negative surface zeta potential for the membranes in a pH range of ca. 3.5–8.0. The fouled membrane classes exhibited elevated negative charges, which were partially restored to the pristine levels when chemically cleaned, suggesting the presence of residual negatively charged foulants. Porosity studies revealed the presence of a porous cake layer with an increase of average pore size and pore volume, and a decrease of 10–20 % on the BET surface area of the fouled membranes. Presence of key compounds on the membrane surface and structure was confirmed via EDX and FT-IR spectroscopy. Surface roughness along with SEM microscopy verified the uniform deposition of the foulants with absence of bulky particles. The presence of a cake layer was confirmed via SEM cross-sectional images due to selective thick layer thickness increase of the fouled membranes. Flux differences between the membrane classes can be related to the thickness of the top layer. Flux decreases and flux recovery ratios were also reported over multiple cycles and linked with porosity and other surface properties.

* Corresponding author.
E-mail address: m.r.bird@bath.ac.uk (M.R. Bird).

https://doi.org/10.1016/j.fbp.2023.07.005

Nomenclature

Abbreviations

BET	Brunauer, Emmett and Teller theory.
BJH	Barrett-Joyner-Halenda theory.
C1	First chemical cleaning stage.
C2	Second chemical cleaning stage.
C3	Third chemical cleaning stage.
CFV	Cross-flow velocity (m s^{-1}).
CMP	Conjugated microporous polymer.
F1	First fouling stage.
F2	Second fouling stage.
F3	Third fouling stage.
FD	Flux decline.
FR	Flux recovery.
LNF	Loose nanofiltration.
MMM	Mixed matrix membrane.
MWCO	Molecular weight cut-off.
PBT	Polybutylene terephthalate.
PES	Polyethersulphone.
PET	Polyethylene terephthalate.
PP	Polypropylene.
PWF	Pure water flux.
TUF	Tight ultrafiltration.

Symbols

J	Flux through the membrane (L m^{-2} h^{-1}).
J_{AF}	Pure water flux after rinsing (L m^{-2} h^{-1}).
J_F	Permeate fouling flux during coffee filtration (L m^{-2} h^{-1}).
J_P	Pure water flux of the membrane prior to fouling introduced on the specific filtration cycle (L m^{-2} h^{-1}).
n	Number of filtration cycle.
pH	Potential of hydrogen.
R_a	Arithmetic average height (nm).
R_q	Root mean square roughness (nm).
R_z	Five-point height (nm).
TMP	Transmembrane pressure (bar).

1. Introduction

Membrane filtration processes are widely used as an alternative for purification, concentration and removal of target compounds from liquid extracts in the food and beverage industry, due to the mild conditions and decreased energy costs (Reis et al., 2019). Previous research in our laboratory explored the use of tight ultrafiltration membranes as a fractionation process step for the selective reduction of caffeine from coffee brews while retaining key compounds (Manios et al., 2022). This approach offers the potential of eliminating any extraction step prior to coffee brew extraction, resulting in a more cost-effective, straightforward and environmentally sustainable process for the production reduced caffeine coffee beverages.

Membrane filtration can offer advantages such as mild processing and low operating costs, however great limitations can be faced in industrial applications due to membrane fouling (Antón et al., 2015). Fouling can be defined as the deposition and adsorption of organic and inorganic material, such as particles, solutes or solute macromolecules, into the membrane pores and/or membrane surface (Liu et al., 2019; Pal, 2015). The size of foulants, membrane-foulant and foulant-foulant interactions, membrane microstructure, surface roughness, porosity and charge are some of many factors affecting fouling. Operating conditions such as feed concentration, pH and transmembrane pressure can also influence the severity of fouling (Argyle et al., 2015). Depending on the foulant's nature, membrane fouling mechanisms can be divided in pore blocking, pore constriction and cake formation (Liu et al., 2019). The severity of fouling can decrease significantly the permeate flux, separation efficiency and membrane longevity of a membrane (Li & Chen, 2010). Therefore, fouling mitigation strategies must be explored, such as selection of a suitable membrane material, feed pre-treatment, membrane cleaning and optimization of operating conditions, to increase the membrane longevity and performance.

Cleaning is one of the most common approaches to maintain, extend and recover the performance of a membrane (Leam et al., 2020). Depending on the nature and the severity of the fouling, cleaning can be generally divided as physical- or chemical-based. Physical cleaning methods, including microbubbles, normal flushing, backflushing and ultrasonication, utilizing mechanical forces to dislodge and remove foulants from the membrane surface (Achilli et al., 2009; Li & Elimelech, 2004; Majeed et al., 2016). The effectiveness of these techniques depends on the degree of interaction between the membrane surface and the attached foulants. Chemical cleaning involves the use of chemical agents which react with the foulants, changing their morphology and altering the surface chemistry of the foulant layer (Bartlett et al., 1995; Bird & Bartlett, 2002). Chemical agents can be mainly categorized as alkalis, acids, surfactants or enzymatic (Chen et al., 2003). Various factors such chemistry and concentration of the cleaning agents, contact time, pH and temperature play an important role for an effective cleaning protocol. However, regular use of cleaning agents, and elevated exposure time and temperature, can alter the membrane chemistry and morphology leading to decreased operational life, and ultimately membrane failure (Kallioinen et al., 2016; Muñoz-Aguado et al., 1996).

Membrane surface charge and porosity can be significantly modified during multiple fouling and cleaning cycles altering the membrane performance (Argyle et al., 2015; Virtanen et al., 2020). Surface charge can contribute to the membrane separation efficiency by rejecting, via repulsion, molecules or particles of opposite charges. Additionally, it can contribute to the severity of the fouling, the nature of the foulant deposits and cleanability, depending on the charge relationship and degree of interaction between the membrane surface and foulants (Bhushan & Etzel, 2009). The surface charge of a membrane can be determined electrokinetically, by the measurement of the streaming potential at solid-liquid interface, and therefore, calculation of the zeta potential (Peeters et al., 1999). Membrane porosity is also directly connected with membrane performance and it is highly impacted by fouling. Depending on the size of the foulants, pore wall adsorption can occur decreasing the pore diameter and evidently completely blocking the pore, or membrane surface accumulation creating a cake layer (Sanaei & Cummings, 2017).

Monitoring the surface charge and the porosity of membranes during fouling and cleaning processes provides useful information about the nature of the fouling, membrane-foulant and foulant-foulant interactions, as well as the effectiveness of cleaning strategies. Weis et al. (2005) reported

the alteration of surface charge to increased negative charges during spent sulphite liquor filtration using regenerated cellulose acetate (RCA) and polyethersulphone (PES) membranes, highlighting the inability of the cleaning agents to recover the surface charge to the pristine membrane state, suggesting irreversible adsorption of foulants and/or adsorption of the cleaning agent. Abd-Razak et al. (2021) reported similar surface charge profiles of conditioned RCA membranes, with different molecular weight cut-offs (MWCO), suggesting no clear connection between these membrane properties. All the membranes experienced similar surface charge decrease when fouled during orange juice ultrafiltration. In contrast, cleaned membranes experienced partial recovery of the surface charge, with a decreasing recovery trend as the MWCO increased, suggesting increased presence of irreversible fouling. In the same study, BET surface area measurements revealed the presence of porosity in the cake layer, along with different pore blocking tendencies on the mesoporous area between the membrane classes (Abd-Razak et al., 2021). The formation of a porous fouling layer followed by an increase in the overall pore volume has been also reported, after membrane fouling by black liquor originated from a mixture of hardwood and softwood (Virtanen et al., 2020). The presence of a porous cake layer during fouling experiments was connected with reduced flux decrease, suggesting that the presence of available pores allows further feed transmission though the fouling layer to the membrane.

The present study builds up on a previous work (Manios et al., 2023), evaluating the effect of surface charge and porosity upon coffee brew filtration during multiple operational cycles, using a commercial tight ultrafiltration polyethersulphone (PES) membrane (MWCO 2 kDa) and bespoke loose nanofiltration PES mixed matrix membrane (PSCD) (MWCO 0.5–1 kDa). Flux variations between different filtration stages along with flux recovery (FR) and flux decline (FD) were also evaluated and connected with membrane properties. Surface and compositional characterization was performed using Fourier-transform infrared spectroscopy (FT-IR) and energy dispersive x-ray (EDX). The membrane morphology was examined via AFM analysis, SEM surface and cross-sectional images.

2. Materials and methods

2.1. Feed solution and cleaning agent preparation

Ground coffee (*Hot Lava Java, Bettys & Taylors Group*) was used for the preparation of the feed solution. More specifically, 50 g of coffee grounds were transferred to a glass tank with 5 kg of deionized water (DI) creating a suspension of 1 % w/w. The dispersion was then heated to 90 °C and stirred constantly for 30 min. Coffee brews extracted in a temperature range of 88–93 °C are characterized by balanced astringency and bitterness, well-balanced aroma and bitterness, and increased compound concentrations, such as caffeine and chlorogenic acid (Cordoba et al., 2020). The coffee extract was then pre-filtered using a 25 μm stainless-steel cartridge filter (*Memtech, UK*) to remove the bulky solid suspended particles at 1.5 bar prior to the cross-flow filtration experiments. Sodium hydroxide (NaOH) pellets (*Alfa Aesar*) were used to prepare the cleaning agent solution by creating a 0.5 % w/v NaOH solution in deionized water (pH=13).

Table 1 – Characteristics of GR95PP and PSCD membranes.

Membrane	PSCD	GR95PP
Manufacturer	Fabricated in-house	Alfa-Laval
Selective layer material	PES+CMP	PES
Substrate material	PET/PBT**	PP**
MWCO (kDa)	0.5–1	2
pH operating range	3–13*	1–13
pH cleaning range	5–13*	1–10
Operating pressure (bar)	1–10*	1–10
Operating temperature (°C)	20–50*	5–60
Pure water permeance (L m^{-2} h^{-1} bar^{-1})	13 (± 1)	10 (± 2)

* Tested range, ** PP = polypropylene, PET = poly(ethylene terephthalate), PBT = poly(butylene terephthalate), PES = polyethersulphone

2.2. Membrane characteristics

A commercial polyethersulphone flat sheet membrane with code GR95PP (*Alfa-Laval*) and a bespoke PES flat sheet mixed matrix membrane (PSCD) with a conjugated poly(arylene ethynylene) microporous polymer (CMP) as an additive (Fig. 9S), were used in this study. The characteristics of the membranes are summarized in Table 1. The membranes were cut into circular coupons with surface area of 14.6 cm^2. New commercial membranes were conditioned with 55 °C DI water filtration for 90 min at 9 bar, to remove glycerol coating (Weis et al., 2005). The PSCD membranes were conditioned with DI water filtration at 25 °C for 90 min at 9 bar.

2.3. Filtration system and operational protocol

Fouling and cleaning experiments for three filtration cycles were conducted in a CF047 circular assembly crossflow cell (47 mm diameter) connected to a metering pump (*P200 Hydracell, Wanner International*, US), as previously described (Manios et al., 2022). Each filtration cycle included pure water flux (PWF) for 60 min, coffee filtration (120 min), rinsing (20 min), PWF (20 min), chemical cleaning (20 min), rinsing (20 min) and PWF (20 min) as described previously (Manios et al., 2022). The membranes were conditioned prior to use before the 1st filtration cycle. The temperature was maintained at 25 °C for all the filtration stages except the chemical cleaning where 50 °C was used. The TMP and cross-flow velocity (CFV) were set at 9 bar and 0.044 m s^{-1} for all the stages except rinsing where they were set to 2 bar and 0.1 m s^{-1}, respectively.

2.4. Membrane performance

The flux J (L m^{-2} hr^{-1}) was calculated using Eq. 1:

$$J = \frac{dV}{dt}\frac{1}{A} = \frac{\Delta V}{\Delta t}\frac{1}{A} \quad (1)$$

The flux is calculated over a fixed time period, Δt (h), where ΔV (litres) is the permeate volume obtained over Δt. A (m^2) is the membrane coupon active surface area (filtration area).

The flux decline (FD) was calculated according to Eq. 2:

$$FD = 1 - \frac{J_{F_n}}{J_{P_n}} \quad (2)$$

where J_F is the permeate fouling flux during coffee filtration, J_P is the pure water flux of the membrane prior to fouling introduced for a specific filtration cycle and n is the cycle number.

The flux recovery (FR) was measured according to Eq. 3:

$$FR = \frac{J_{AF_n}}{J_{P_n}} \quad (3)$$

where J_{AF} is the pure water flux after rinsing, J_P is the pure water flux prior to fouling of the membrane introduced for a specific filtration cycle and n is the cycle number.

2.5. *Membrane characterization*

2.5.1. *FT-IR – chemical structure analysis*

The FTIR spectra of coffee powder, GR95PP and PSCD membranes were obtained using a Spectrum 100™ – FTIR Spectrometer (*PerkinElmer*, USA) fitted with an attenuated total reflectance (ATR) accessory. A background scan was run prior to sample testing and spectra were recorded from 4000 to 650 cm^{-1} in transmission mode with a spectral resolution of 4 cm^{-1} and 32 scans. Thin slices of the membranes and ground coffee powder were directly measured. The samples were dried at least for 24 h at room temperature prior to analysis.

2.5.2. *Scanning electron microscope (SEM)*

Scanning electron microscope (SEM) was used to observe the state of membrane surface and cross-section for different membrane conditions: Conditioned, fouled and cleaned. Air and vacuum-dried membranes were glued onto SEM stubs using conductive paste, followed by coating with a thin layer of chromium. The chromium-coated samples were them imaged using a JSM 6480LV SEM (JEOL Ltd, Japan). The elemental composition of the different membrane surfaces was evaluated via energy dispersive X-ray (EDX) coupled with the SEM.

2.5.3. *Atomic force microscopy*

The topography and roughness of the membrane surfaces were determined via AFM. The measurement was performed using a Multimode AFM (Veeco Metrology, USA) with a Nanoscope Analysis 1.7 software. The cantilever was used in contact mode with silicon soft tapping mode tips (Tap150AI-G, Budget Sensors, Bulgaria). Images were scanned at 1 µm × 1 µm scan size at a rate of 1 Hz for conditioned, fouled and cleaned membranes. The program software Gwyddion *(Czech Metrology Institute, CZ)* was utilized for result analysis.

2.5.4. *Surface charge*

The measurements of the zeta potential of GR95PP and PSCD membranes were carried out using an Electrokinetic Analyzer (*SurPASS, Anton Parr*, Graz, Austria), using a 0.001 M potassium chloride (KCl) solution as the electrolyte solution. The pH range covered was 3–8. The solution pH was first shifted to pH 8 using a dilute KOH solution and then automatically titrated from pH 8–3 using 0.05 M HCl solution, during the analysis.

2.5.5. *Porosity analysis*

Membrane surface areas and pore size distributions were measured by nitrogen adsorption and desorption at 77 K using a Micromeritics 3Flex volumetric gas sorption analysis system. The specific surface area was calculated according to the British Standard guidelines for the BET method from regression analysis of data in the relative pressure range from 0.05 to 0.3, using the manufacturer-recommended equilibration period (Institution, 1996). Pore size, pore volume and pore size distributions were derived from the desorption branches of the isotherms (Fig. 7S, Fig. 8S) using the Barret, Joyner and Halenda (BJH) method and the reference curve for Harkins-Jura (Barrett et al., 1951; Harkins & Jura, 1944), as previously reported (Virtanen et al., 2020). A membrane sample with mass of 100 mg per filtration stage was used. Dried membrane samples were cut into small pieces and degassed at 40 °C for 4–8 h under vacuum before analysis.

3. Results and discussion

3.1. *Surface zeta potential*

The effect of fouling and cleaning on the surface zeta potential of the PSCD and GR95PP membranes versus the pH was investigated for the conditioned, fouled once (F1), cleaned once (C1) and fouled twice (F2) membranes. AgCl electrodes coating appear to have reduced chemical stability in alkaline environment for pH values above 8, Also, an acidic environment for pH values below 3 can prevent accurate measurements due to the development of greater conductivity. Consequently, the zeta potential was investigated in the range of pH 3–8 (Wu & Bird, 2007).

The zeta potential of PSCD membranes in different filtration stages is presented in Fig. 1. The conditioned membrane had a negative charge in the range of pH 3.5–8.0 and positive charge in the range of $3.0 \leq pH < 3.5$, with the isoelectric point at pH 3.5. After the 1st fouling stage (F1), the zeta potential values decreased significantly with the isoelectric shifting higher to pH 4.0, increasing the positively charged range of the membrane. Additionally, the membrane surface zeta potential become more sensitive to pH variations. Protein and polyphenol compounds found on the coffee brews exhibit elevated negative charges in this pH range (Zhang et al., 2016) Their presence on the fouled membrane was verified by FT-IR and EDX analysis, explaining partially the surface charge change (Fig. 3, Table 1S).

The cleaned membrane after the 1st cycle exhibited less negative zeta potential values compared to the fouled membrane (F1), but remained more negatively charged than the conditioned state. The presence of foulants after the 1st cleaning cycle was confirmed by FT-IR and EDX (Fig. 3, Table 1S) explaining the partial restoration of the surface charge to the conditioned membrane. Finally, the zeta potential of the membranes was shifted again to more negative values after the 2nd fouling stage (F2) which can be attributed to the negative nature of the foulants. Interestingly, the surface zeta potential was less negatively charged compared to the F1 in the pH range of 4.5–8 and the isoelectric point was between the conditioned and fouled once membrane. This could be attributed to the increased negative charge of the cleaned membrane (compared to the conditioned) which acted as a repulsion barrier for a part of negatively charged foulant depositions during the 2nd fouling stage.

The surface zeta potential of the GR95PP membranes in the conditioned, F1, C1 and F2 states was also investigated (Fig. 1). The conditioned membrane exhibited negatively charged surface for pH values 4.5–8.0, with the isoelectric point found at approximately pH 4.2. The membrane exhibited positive zeta potential values in the pH range 3.0–4.2. Following the 1st fouling stage (F1), the surface zeta potential shifted to more negative values in the pH range of 4–8,

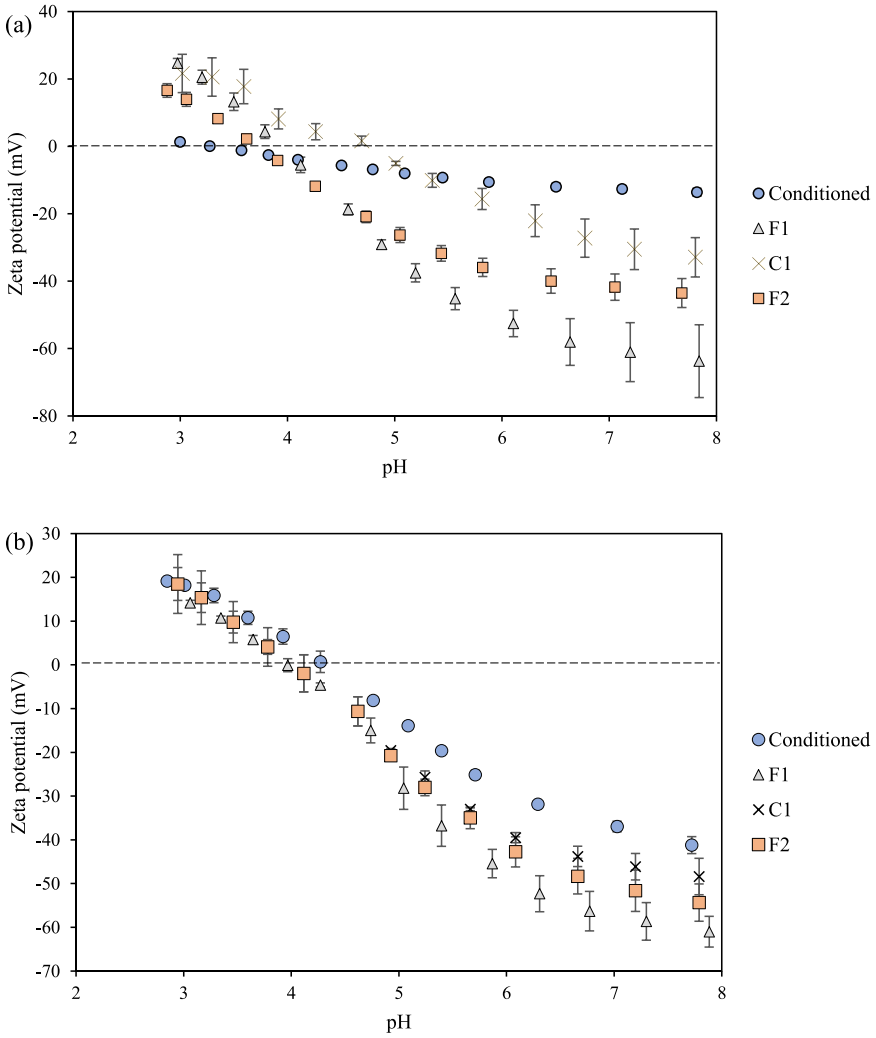

Fig. 1 – Zeta potential (mV) versus pH of the (a) PSCD and (b) GR95PP membranes after conditioning, 1st fouling (F1), 1st cleaning (C1) and 2nd fouling (C2) stages.

attributed to the presence of foulants as discussed above for the PSCD membranes. The isoelectric point also slightly shifted to pH 4. Below this value, the membranes exhibited approximately similar positive values with the conditioned membranes, reaching a maximum voltage of + 14 mV. Chemical cleaning of the membrane decreased the surface charge to less negatively charge values compared to the fouled membrane, however the membrane remained more negatively charged than the conditioned one, suggesting the residual presence of foulants after the cleaning step. The surface charge remained similar as the fouled membrane for pH values below 4.7, where the isoelectric point experienced no significant change. Finally, after the 2nd fouling stage the surface zeta potential decreased to more negative charges for pH 4.9–8.0, however it remained between the conditioned membrane and once fouled (F1) analogues.

Comparing the two membranes, the GR95PP membranes were more negatively charged than the PSCD membranes in their conditioned state despite being fabricated from the same polymer. PES membranes exhibit increasing negative charges as the casting solution concentration increased due to the increased density of sulfonyl and ester groups (Al Malek et al., 2012). Additionally, the presence of additives such as polyvinylpyrrolidone (PVP) increases the negative charge of the PES membranes (Susanto & Ulbricht, 2009). It is postulated that the commercial membranes were fabricated with higher casting concentrations compared to the PSCD membranes with the possible presence of PVP, however such information is not available in the public domain. Moreover, the presence of the non-polar additive in the PSCD membrane could shift the surface zeta potential to less negative charges, enhancing the charge difference between the membranes. Both membranes exhibited the same behaviour to the different fouling and cleaning stages, with the PSCD membranes affected more intensively in terms of zeta potential differences and isoelectric point variations. These differences could be attributed to the initial enhanced negative charge of the GR95PP membranes which acted as a stronger repulsion barrier for surface charge modifications.

3.2. *Porosity analysis*

The BET surface area, total pore volume and desorption pore size of the PSCD and GR95PP membranes for three consecutive filtration cycles for the conditioned, fouled and cleaned states were examined (Table 2). Surface area wise, the PSCD membranes exhibited a decreasing trend as the membrane became fouled for all the filtration cycles, attributed to the blockage of pores. In contrast, the total pore volume increased after the fouling stages (F1, F2, F3), which can be attributed to the presence of porosity in the fouling layer.

The decrease of the BET surface area and increase of the pore volume, corresponds to the average pore size, where a shift to much higher pore sizes was observed when the membranes became fouled. This shift could explain the decrease of the surface area, where small pores were blocked and at the same time the foulant layer appeared, with larger pore porosities shifting the overall pore size to higher values. The surface area returned to similar values compared to the conditioned state after the membranes underwent chemical cleaning where the membrane after 1st cleaning exhibited the smallest change. The partial restoration of the pore volume could be attributed to the presence of foulant porosity and dead-end blocked pores which cannot be restored to the conditioned state. Finally, the pore size reduced to values closer to the conditioned membrane, indicating a removal of the foulant layer in combination with the unclogging of smaller diameter pores.

Similar decreasing trend on the BET surface area for the GR95PP membranes was observed after fouling, suggesting pore blockage. The total pore volume slightly increased for the fouled membranes which comes in accordance with the PSCD membrane results, suggesting the existence of porosity in the foulant layer and in combination with the increase in the desorption pore size, it suggests the blockage of small pores and at the same time, porosity of the foulant layer which shifts the overall pore size to higher values. After cleaning, the GR95PP membranes experienced an increase in surface area to values close to those of the conditioned analogue, showing restoration of a portion of the pores in their initial state. The total pore volume was reduced when the membranes were cleaned; however an increasing trend was observed as the cleaning cycles progressing. These results are in accordance with the pore size data, where the membrane pore size was decreased when the membranes was cleaned. The membrane pore size steadily increased during the build-up of foulant material as the filtration cycles were progressing.

To further understand the impact of fouling and cleaning on membrane porosity, pore area and pore volume distributions for both membranes were obtained in the range of 2–80 nm for the conditioned, F1, C1, F2, C2, F3 and C3 states (Fig. 2, Fig. 1S). Both membranes in the conditioned state exhibited presence of pores in the mesoporous (2–50 nm) and macroporous (> 50 nm) regions (Matthias et al., 2015). The conditioned GR95PP membranes exhibited pore areas in the ranges of 2–8 and 10–80 nm, whereas the PSCD analogues exhibited an overall lower surface area in the same range. For both membranes, the sharp intense peak at approximately 3.7 nm was attributed to the tensile strength effect (TSE) which occurs due to the cavitations between pores that create an interconnected pore system (Groen et al., 2003; Lai et al., 2020). For this reason, the pore distributions generated by the adsorption branch must be investigated to verify the presence of this peak since it is not affected by TSE phenomenon (Groen et al., 2003). The adsorption branch pore area distribution revealed the presence of porosity around 3.7 nm. However, this displayed much lower intensity, suggesting that a significant fraction of the intensity displayed is an artifact due to the phenomenon described above.

After the 1st cycle fouling (F1), the GR95PP membranes exhibited a decrease in the pore area in the range of 2–60 nm indicating that the decrease in the BET surface area of the membrane could be also connected to the fouling of pores in this range (Fig. 2a). A similar decrease in the pore volume was observed in the range of 2–60 nm indicating pore clogging (Fig. 2b). Since an increase of the total pore volume was observed for the fouled membranes, along with increase in the average pore size, it is postulated that the porosity introduced from the fouling layer was in the macroporous range (> 60 nm). PSCD membranes exhibited a decrease in the surface area of the pores, mostly in the range of 2–10 nm (Fig. 1S) for the 1st filtration cycle. The volume also decreased in the range of 2–60 nm, indicating that the overall pore volume increase could be attributed to the macroporosity introduced from the fouling layer.

Table 2 – BET surface area, cumulative pore volume and average desorption pore size based on nitrogen adsorption–desorption isotherms for the PSCD and GR95PP membranes for three filtration cycles.

Membrane	Cycle stage	BET surface area (m^2/g)	Total pore volume (cm^3/g)	Desorption pore size (nm)
PSCD	Conditioned	5.44	0.054	38
	F1	4.78	0.105	72
	C1	4.93	0.097	63
	F2	4.39	0.096	65
	C2	5.47	0.081	44
	F3	4.21	0.109	78
	C3	5.61	0.095	77
GR95PP	Conditioned	9.76	0.087	33
	F1	7.97	0.104	45
	C1	9.67	0.089	33
	F2	8.07	0.102	41
	C2	9.16	0.095	38
	F3	8.28	0.104	42
	C3	9.15	0.101	41

Both membranes exhibited similar pore surface and volume distributions for the conditioned state, however it was observed that there was no complete regeneration of the membranes to their initial state. PSCD membranes exhibited lower pore area and volume compared to GR95PP, which can be partially attributed to MWCO differences. Similar behaviour was observed during the fouling and cleaning stages for both membranes and for all filtration cycles, with small variations in the pore area and volume between the membrane states.

3.3. *Membrane surface analysis*

FT-IR spectroscopy was used to identify the presence of key compounds, polyphenols, proteins and caffeine, in the membrane structures of the PSCD and GR95PP membranes throughout three filtration cycles (Fig. 3, Fig. 2S, Fig. 3S). More specifically, the coffee protein symmetric -CH_3 bending of the methyl groups was found in broad low intensity bands at 1350–1390 cm^{-1} (Zhang et al., 2016) for all the fouling stages for the PSCD membranes (Fig. 3c). After cleaning, the band intensity decreased for the 1st and 3rd cycle suggesting the presence of residual protein, in contrast with the cleaned membranes in the 2nd cycle where the band intensity remained similar to the conditioned one. Caffeine -C═O stretching vibrations were also observed at 1653 cm^{-1} (Butt et al., 2019) after the membranes were fouled (Fig. 3, Fig. 3S). After the 1st fouling cycle, the membranes exhibited a large peak which then decreased for the 2nd and 3rd cycles. Although there was a decrease in the peak intensity, this

remained significant, suggesting the presence of foulant layer rich in caffeine on the membrane surface for all filtration cycles. After cleaning, the intensity of the peak decreased yet remained significant, indicating a residual presence of caffeine. Finally, the -OH stretching at 3330 cm^{-1}, which corresponds to polyphenols (Flores-Valdez et al., 2020), was observed for all the fouled membranes for all the filtration cycles (Fig. 3). The presence of residual polyphenols was also observed on cleaned membranes.

Polyphenol build up was also observed for the GR95PP membranes (Fig. 2S), with a similar profile as for the PSCD membrane. A difference between the two was the peak in the 1st fouling cycle attributed to the presence of an excess glycerine coating as discussed previously (Manios et al., 2022). After cleaning, the membranes exhibited lower intensity peaks compared with the fouled analogues, however an increasing trend was observed, indicating polyphenol build up, even after cleaning. Protein presence was observed in all the fouling stages with similar band intensities verifying their presence in the foulant layer for all the cycles. Interestingly, the 1st cycle cleaned membrane exhibited almost complete elimination of this band, in contrast with the 2nd and 3rd fouling stage where the intensity decreased, however it remained in similar levels with the fouled analogues, indicating presence of protein molecules on the cleaned membrane structure. Finally, the presence of caffeine was verified on the fouled membranes with similar peak intensities (Fig. 3S). The cleaned membranes exhibited an increasing trend of caffeine presence as the cycles progressed until the 2nd cycle, showing a further build-up of caffeine, however on the 3rd cycle, the stretching vibrations were slightly decreased compared to the fouled analogue.

No clear trend for key compound accumulation was observed for either membrane as the cycles progressed after the fouling stages. However, the PSCD membranes exhibited a higher recovery compared to the conditioned stage when cleaned, showing decreased peak intensities for all the cycles. A higher recovery for the PSCD membranes could be partially attributed to the increased recovery of the surface charge of the membrane after cleaning. The lower surface charge of the conditioned and cleaned membranes could affect the membrane-foulant interaction, decreasing the level of adhesion of organic carbons and other ionically charged foulants to the membrane surface (Ba & Economy,

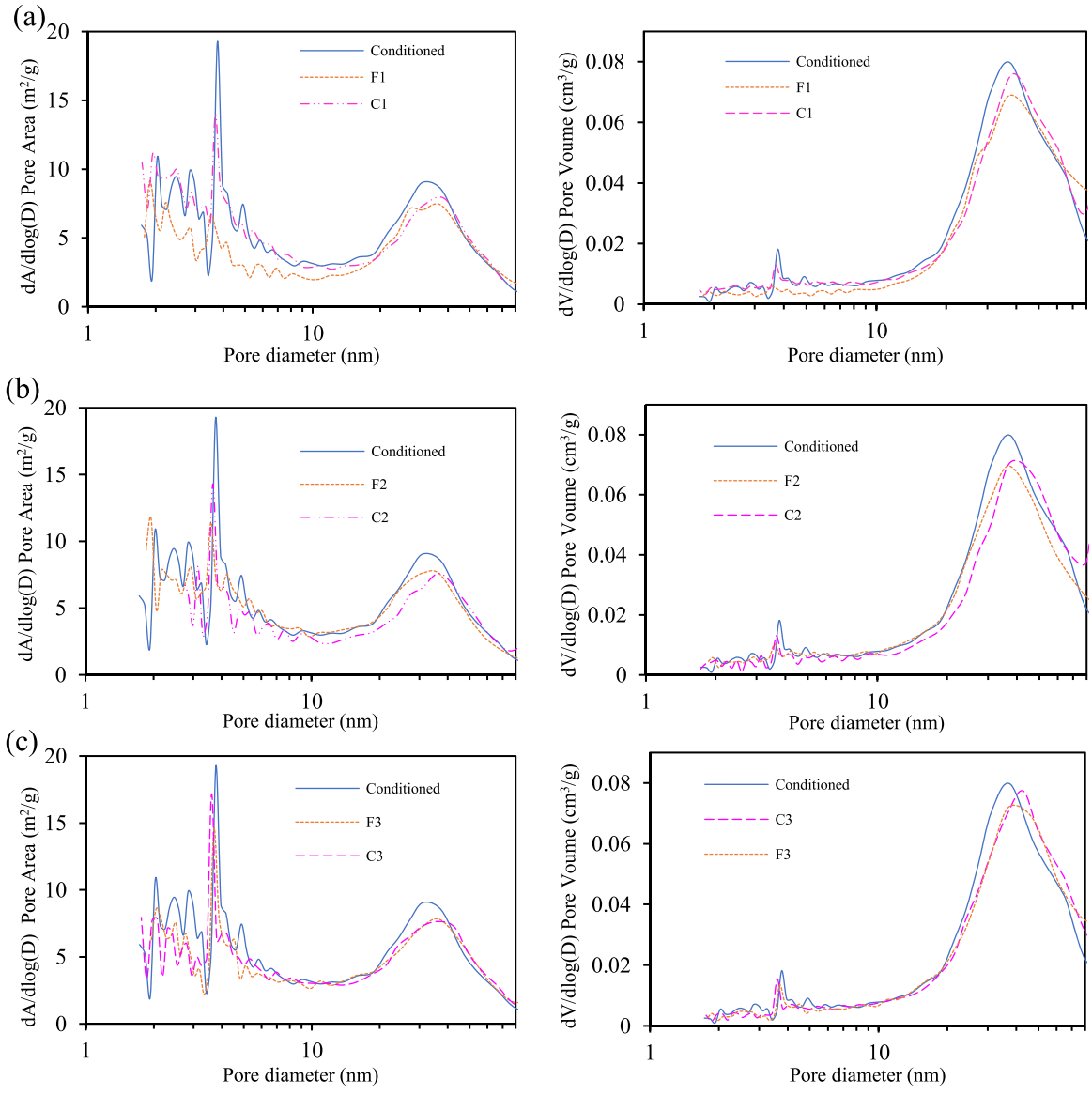

Fig. 2 – BJH pore area and pore volume distributions of GR95PP membranes for the 1st (a), 2nd (b) and 3rd (c) filtration cycle of coffee brews.

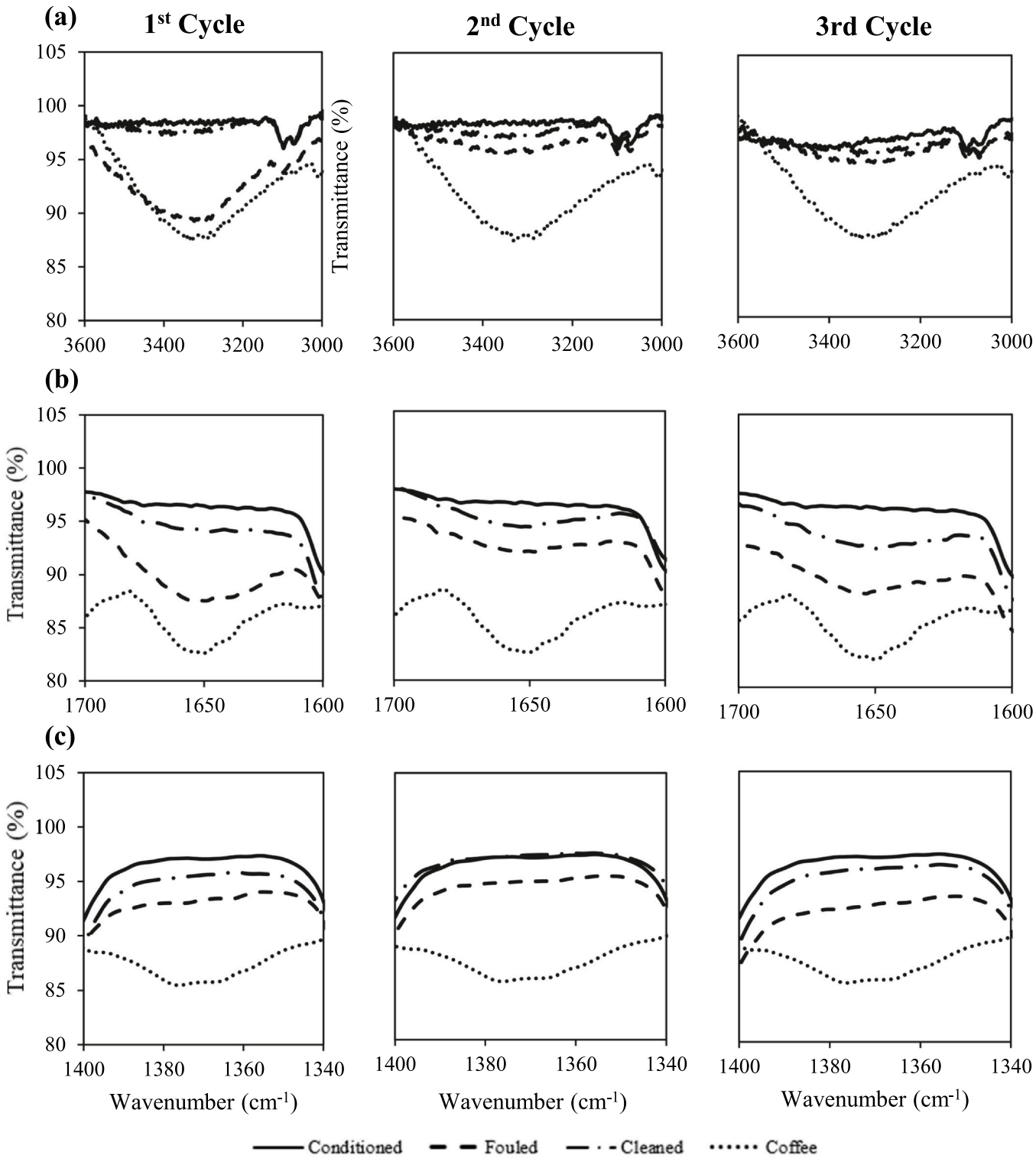

Fig. 3 – FT-IR spectra of coffee and PSCD membranes during three filtration cycles for (a) polyphenols, (b) caffeine and (c) proteins.

2010). In contrast, GR95PP exhibited an increasing trend of compound presence for the cleaned membranes compared to the fouled analogues (with the exception of the 1st cycle) (Fig. 2S). More specifically, for caffeine and protein, the band/peak intensity of the cleaned membranes in the 2nd cycle was slightly lower compared to that of the fouled membranes.

On the 3rd cycle, the intensity of the peaks was found to be almost the same between the two states. These results indicate that saturation of the membranes can be occurring for caffeine and proteins, where small intensity differences are observed between the fouled and cleaned states.

Elemental analysis of the membrane surfaces allowed the extraction of compositional information concerning the nature of the fouling (Table 1S). Since both membranes were fabricated with polyethersulphone, the presence of C, O and S on the conditioned membrane surfaces was to be expected. GR95PP membranes exhibited a higher oxygen content which can be attributed to the residual glycerol which was not removed during the conditioning step. PSCD membranes

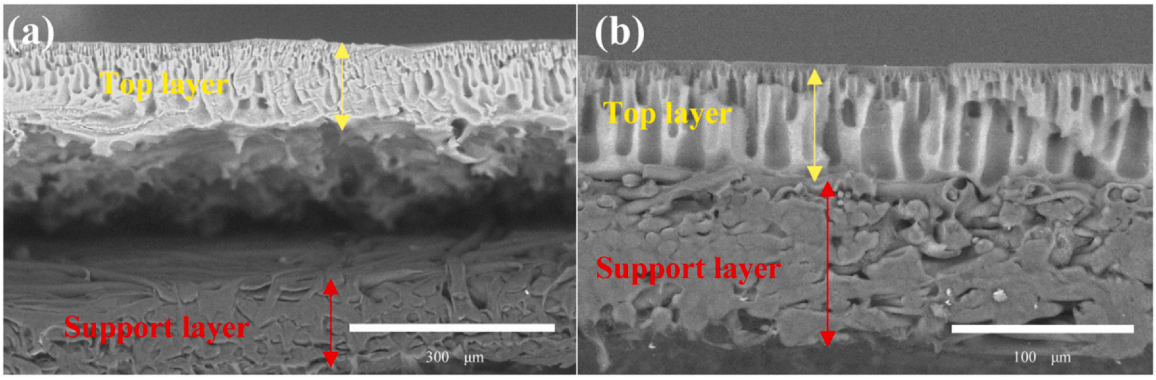

Fig. 4 – FE-SEM cross-section micrographs of the overall cross-section of the GR95PP and PSCD membranes.

exhibited higher carbon content, which can be attributed to the presence of the poly(aryleneethynylene) conjugated microporous polymer as an additive, which consisted solely of carbon and hydrogen atoms (Fig. 9S).

After introducing the membranes to the 1st fouling stage (F1), the appearance of nitrogen in the surface composition was observed and linked to the deposition of nitrogen-rich caffeine and proteins, in accordance with the FT-IR findings (Figs. 3, 2S). Additionally, the presence of elements such as Al, Si, K, Cl, Na was observed in low percentages summing to a total of 1.4 and 1.3 wt%, for PSCD and GR95PP respectively. These elements can be found in small concentrations in coffee infusions (Krivan et al., 1993; Martín et al., 1998; Zaidi et al., 2005). The presence of Al can be also originated from the aluminium stub used for analysis (Abd-Razak et al., 2019). A significant decrease in the carbon content was observed for the PSCD membranes along with a slight increase for the oxygen. This change can be attributed to the presence of polyphenols, proteins and caffeine on the foulant layer, since all these molecules contain multiple hydroxyl and/or carbonyl groups, along with the higher precentange of carbon for the bespoke membrane. Following the 1st cleaning stage, both membranes experienced a decrease in nitrogen weight content, in accordance with the FT-IR findings. The carbon and oxygen content for the PSCD membranes was restored to values similar to those of the conditioned membrane, showing the effectiveness of the cleaning regime. GR95PP membranes exhibited no significant compositional changes in these elements.

A similar trend was observed for both membranes in the 2nd fouling stage (F2) and 2nd cleaning stage (C2) where nitrogen content increased during the fouling stages and then decreased after cleaning, showing presence of residual caffeine and protein on the membrane surface. The PSCD and GR95PP membranes also exhibited a similar trend for the carbon and oxygen content. The nitrogen content remained stable for both membranes in the 3rd fouling (F3) and 3rd cleaning (C3) stages, in agreement with the FT-IR findings, where both membranes exhibited a slightly decreased peak intensity for the cleaned membranes.

Overall, the presence of key compounds was confirmed for both membranes thoughout the fitlration cycles, highlighting their contribution to the membrane fouling. Higher recovery during cleaning for PSCD membranes was connected and partially attributed to surface charge differences. Neither membranes exhibited a clear trend in the fouling stages in terms of compound build up.

3.4. *Membrane morphology*

Scanning electron microscopy (SEM) and field emission scanning electron microscopy (FESEM) was used to monitor the cross-sectional morphology and thickness of the GR95PP and PSCD membranes (Fig. 4, Fig. 4S). Both membranes have an asymmetric structure consisting of a porous support layer and top skin layer GR95PP membranes have a polypropylene fibrous support layer with a thickness of approximately 130 (± 8) μm and a top layer made of polyethersulphone (PES), with a thickness measured at 132 (± 6) μm. For the fabrication of the PSCD membranes, a PET/PBT porous substrate and a PES top layer with thicknesses 100 (± 4) and 70 (± 2) μm, respectively, were used. The measured thickness of the substrate was slightly lower than the specifications provided from the supplier (120 μm) and this could be attributed to compaction due to the membrane conditioning under elevated pressures (Persson et al., 1995).

The PP substrate was easily delaminated during the sample preparation stages for SEM and zeta potential measurements suggesting moderate adhesion between the layers, in contrast with PSCD membranes where no delamination was observed. Comparing the top layer of the membranes, a thickness difference of approximately 50 μm was observed. This can partially explain the pure water flux difference of the conditioned membranes. The difference in the thicknesses between the membranes can be attributed to higher polymer concentrations used in the casting solutions for the GR95PP membranes (Kluge et al., 2022). This could also explain the higher negative surface charge of the commercial membranes against the in-house fabricated ones, due to increased charged group density, as previously discussed. No structural degradation was observed for the top layer during the fouling and cleaning stages when samples were compared to the conditioned membranes (Fig. 4S).

The thickness of the selective skin layer was measured for all the fouling and cleaning stages for three consecutive cycles along with the conditioned analogues (Table 3). Comparing the two classes of membranes, a significant thickness difference was observed, of 0.22 μm and 2.1 μm in their conditioned state, for PSCD and GR95PP membranes respectively. Both membranes, exhibited an increase in their thickness when fouled in the first cycle, suggesting the formation of a thin cake layer, as supported by the porosity analysis. Following the cleaning stage, the thickness decreased for the both membranes, suggesting the removal of the cake layer. A similar trend was observed for both

Table 3 – Thickness of the selective thin skin layer of the PSCD and GR55PP membranes after fouling and cleaning for three consecutive filtration cycles.

	Thickness (μm)						
	Conditioned	F1	C1	F2	C2	F3	C3
GR95PP	2.1 (± 0.3)	3.0 (± 0.6)	2.0 (± 0.4)	2.7 (± 0.5)	1.9 (± 0.3)	2.9 (± 0.6)	1.9 (± 0.4)
PSCD	0.22 (± 0.03)	0.33 (± 0.08)	0.24(± 0.02)	0.30 (± 0.05)	0.24 (± 0.02)	0.32 (± 0.07)	0.23 (± 0.02)

membranes, where the thickness varied between the fouling and cleaned membranes values for the 2nd and 3rd cycle. The thickness values for the fouled states for both membranes experienced a higher deviation from the mean value, which could be attributed to insignificant thickness deposit variations of the foulant deposits between different areas of the membrane surface.

To aid a further understanding of the changes in surface morphology throughout the filtration cycles, atomic force microscopy (AFM) for the conditioned, fouled and cleaned membranes was used (Table 2S). The PSCD membranes exhibited a no clear trend for the roughness R_a mean values when the membranes were fouled, since any variations were considered negligible since they lied mostly in the error margin. The R_q values, which are more sensitive to peak and valley presence, indicated a decreasing trend for the surface roughness of the membranes when they were fouled, suggesting that the foulants were uniformly deposited on the membrane surface creating either even surfaces or reducing the intensity of peaks and valleys (Gadelmawla et al., 2002). The R_z parameter provides the difference between the five highest and five deepest valleys, and showed that the fouled membranes exhibited slight decrease suggesting that the foulants were potentially mostly deposited inside formed valleys, filling surface cavities (Dizge et al., 2011). A similar trend was observed for the fouled GR95PP membranes, where a slight decrease in the roughness parameters was observed. The cleaning step showed recovery of the surface roughness for both membranes over the three filtration cycles, not compromising their surface integrity. Comparing the two membrane classes, they both exhibited low surface roughness values in their conditioned state which could contribute to the reduced possibility of bulky foulants entrapment, along with parameters such as cross-flow velocity and composition of the stream (Manios et al., 2022).

Surface investigation via SEM micrographs was conducted for the conditioned, fouled and cleaned GR95PP and PSCD membranes for three consecutive filtration cycles (Fig. 5S). The conditioned PSCD membranes appear to have a smooth surface whereas the GR95PP membranes have an etched surface which can be attributed to the fabrication procedure and/or the sampling procedure. No presence of bulky foulants nor deposits was observed for either membranes for all the fouled stages, indicating that the foulants were likely deposited uniformly on the membrane surface subsequently to pore entrapment. These results come in accordance with the AFM findings where the surface roughness exhibited an insignificant decrease when the membranes were fouled, suggesting potentially cavity deposition. The cleaned membranes exhibited no clear deterioration or deformation, indicating that the cleaning agent along with the cleaning conditions did not compromise the surface integrity of the membranes. The appearance of etching on the PSCD membranes was attributed to the sampling procedure.

Overall, significant membrane top layer thickness differences were observed, partially explaining the surface charge differences seen between the membrane classes, due to potential compositional casting variation. The presence of a thin foulant layer was confirmed for both membranes due to selective layer thickness differences which were largely removed. AFM suggested cavity and/or uniform deposition of the foulants for both membranes, in accordance with SEM surface investigations where an absence of bulky deposits was observed. No structural degradation from a surface or cross-section perspective was observed for either membrane.

3.5. *Flux analysis*

Fig. 6S presents the permeate flux of the GR95PP and PSCD membranes measured for the conditioned, fouled, rinsed and cleaned states for three consecutive cycles. Transmembrane pressure and operational temperature of 9 bar and 25 °C, respectively, were used as operating conditions in the cross-flow set-up. The pure water flux (PWF) of the PSCD and GR95PP membranes were around 84 and 58 $L\,m^{-2}\,h^{-1}$, respectively. Both membranes exhibited negative surface charge in neutral pH (pH of the DI water used for the experiments). Since no solutes were present in the PWF experiments, surface charge was a poor indicator for the permeate flux difference. The GR95PP membranes exhibited higher pore volume and areas in the mesoporous range compared to the PSCD membrane, in agreement with the higher MWCO of the commercial membranes. Thus, it would be expected that the commercial membranes would exhibit a higher water permeate flux, however the opposite was observed. Nonetheless, the commercial membranes exhibited much higher top layer and selective skin layer thickness compared to the PSCD, explaining the permeate flux differences. Additionally, the increased porosity of GR95PP membranes could be also attributed to the presence of 'dead' pores, that do not contribute to the overall membrane flux.

The permeate flux decreased significantly for both membranes when fouled for the 1st filtration cycle fouling stage, with a flux decline (FD) of 86 % and 90 % on the 1st cycle for the PSCD and GR95PP membranes respectively (Fig. 5). These results are in agreement with the decrease in porosity in the range of 2–60 nm (Fig. 2, Fig. 1S) and the negative shift in surface zeta potential (Fig. 1). This suggested the presence of negatively charged substances also deposited on the membrane surface. A boundary layer with high concentration of negatively charged compounds could be also created across the membrane surface, contributing to the reduction of the transmembrane flux due to concentration polarization (Luis, 2018). The flux decline increased to 92 % and 94 % for PSCD and GR95PP membranes for the 2nd cycle, respectively. These results indicate that the surface charge change of the cleaned membrane was not sufficient to improve the flux performance even though the membranes exhibited a

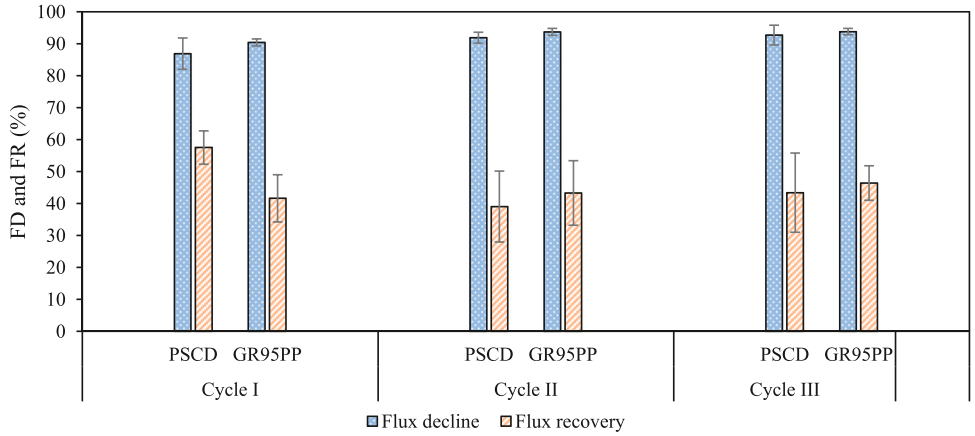

Fig. 5 – Flux decline and flux recovery for the PSCD and GR95PP membranes for three consecutive filtration cycles.

slightly increased negative charge after cleaning. Similar values for the 3rd cycle were observed, exhibiting a steady state trend.

Flux recovery (FR) ratio was used to estimate the efficiency of physical cleaning and the foulant nature (Fig. 5). The commercial GR95PP membranes exhibited FR ca. 43 % for all the filtration cycles suggesting that chemical cleaning must be introduced to remove remaining foulants. The PSCD membranes exhibited a higher FR of 58 % for the 1st cycle rinsing, however this was reduced to ca 40 % for the 2nd and 3rd filtration cycles. These results indicate pore entrapment of foulants for both membranes, and the possible existence of a remaining cake thin layer, which could not be removed by shear forces. Both membranes exhibited higher PWF after chemical cleaning compared to the PWF of the conditioned membranes, showing efficient regeneration of the membranes, flux-wise (Fig. 6S). The elevated flux may be attributed to the adsorption of elements from the cleaning agent as previously described (Manios et al., 2023; Weis et al., 2003). The cleaned membranes exhibited similar flux values for all the cycles for GR95PP and a negligible increase from the 1st to 2nd cycle for the PSCD membranes where the flux remained similar after cleaning for the 3rd filtration cycle. Since porosity results suggested partial restoration of mesopores after cleaning, these results suggested only a portion of these pores are active, and that the presence and blocking of dead pores had also occurred.

Overall, PSCD membranes exhibited higher PWF values connected mainly to top layer thickness differences. Both membranes exhibited similar FD and FR values throughout the filtration cycles. Consideration of chemical cleaning along with porosity studies for both membranes revealed the presence of clogged ‘dead’ pores in each case, as fluxes were effectively restored despite only a partial restoration of porosity occurring.

4. Conclusions

Surface charge and porosity variations of GR95PP and PSCD membranes were investigated, along with morphology and surface properties for three consecutive coffee brew filtration cycles. Both membranes exhibited negative surface zeta potentials over the pH range of operation. Surface charge after fouling shifted to further negative charges for both membranes, with the charge recovering partially after cleaning, revealing the presence of residual negatively charged foulants. PSCD membranes revealed lower surface charge and with higher charge variations between the cycles. Porosity analysis revealed the presence of a porous fouling layer which increased the average pore size of the membranes, experiencing a minor decrease in their surface area due to the blockage of mesopores. GR95PP membranes exhibited higher pore areas and volumes compared to PSCD membranes, partially explaining the MWCO differences. Surface analysis confirmed the presence of proteins, caffeine and polyphenols on the membranes after fouling, along with the presence of residual quantities of these compounds after cleaning, suggesting their involvement in surface charge, porosity differences and flux variations. Compositional studies also showed the presence of element traces originating from the coffee brews. AFM revealed a relatively uniform deposition of the foulants on the membrane surfaces reducing their overall roughness. The absence of bulky deposits was confirmed by surface investigation using SEM. Cross-section image investigation revealed a significant difference in the top layer thickness of the membranes, explaining differences in flux performance between the membrane classes. Selective skin layer thickness was also monitored along the filtration cycles, showing presence of deposits and formation of thin foulant layers. No structural alteration due to the filtration cycles were observed. Finally, surface charge proved to be a poor indicator of flux variations. Both membranes exhibited similar flux declines, despite the MWCO difference, linked mainly to pore blockage and the formation of cake layers. Physical cleaning provided partial flux recovery for both membranes, suggesting the implementation of an effective chemical cleaning protocol. Sodium hydroxide was found to be effective in restoring the membranes flux, despite porosity studies revealed only partial regeneration of pores in the mesopore range, suggesting presence of blocked ‘dead’ pores.

Declaration of Competing Interest

The authors declare that they have no known competing financial interests or personal relationships that could have appeared to influence the work reported in this paper.

Acknowledgements

We thank our industrial collaborators: Andrew Downie of *Bettys & Taylors Group, UK* for the supply of coffee, and David Carr of *Kerry Ingredients, Cam Gloucestershire* for the supply of dead-end prefiltration cartridges. DM acknowledges EPSRC,

UK for support (grant EP/V047078/1). We also like to thank Dr. Hannah Leese from the *Department of Chemical Engineering, University of Bath* and the Materials micro-mechanical facility, *University of Bath* for performing the AFM analysis.

Appendix A. Supporting information

Supplementary data associated with this article can be found in the online version at doi:10.1016/j.fbp.2023.07.005.

References

Abd-Razak, N.H., Chew, Y.M.J., Bird, M.R., 2019. Membrane fouling during the fractionation of phytosterols isolated from orange juice. Food Bioprod. Process. 113, 10–21. https://doi.org/10.1016/j.fbp.2018.09.005

Abd-Razak, N.H., Pihlajamäki, A., Virtanen, T., John Chew, Y.M., Bird, M.R., 2021. The influence of membrane charge and porosity upon fouling and cleaning during the ultrafiltration of orange juice. Food Bioprod. Process. 126, 184–194. https://doi.org/10.1016/j.fbp.2021.01.009

Achilli, A., Cath, T.Y., Marchand, E.A., Childress, A.E., 2009. The forward osmosis membrane bioreactor: a low fouling alternative to MBR processes. Desalination 239 (1), 10–21. https://doi.org/10.1016/j.desal.2008.02.022

Al Malek, S.A., Abu Seman, M.N., Johnson, D., Hilal, N., 2012. Formation and characterization of polyethersulfone membranes using different concentrations of polyvinylpyrrolidone. Desalination 288, 31–39. https://doi.org/10.1016/j.desal.2011.12.006

Antón, E., Álvarez, J.R., Palacio, L., Prádanos, P., Hernández, A., Pihlajamäki, A., Luque, S., 2015. Ageing of polyethersulfone ultrafiltration membranes under long-term exposures to alkaline and acidic cleaning solutions. Chem. Eng. Sci. 134, 178–195. https://doi.org/10.1016/j.ces.2015.04.023

Argyle, I.S., Pihlajamäki, A., Bird, M.R., 2015. Black tea liquor ultrafiltration: effect of ethanol pre-treatment upon fouling and cleaning characteristics. Food Bioprod. Process. 93, 289–297. https://doi.org/10.1016/j.fbp.2014.10.010

Ba, C., Economy, J., 2010. Preparation and characterization of a neutrally charged antifouling nanofiltration membrane by coating a layer of sulfonated poly(ether ether ketone) on a positively charged nanofiltration membrane. J. Membr. Sci. 362 (1), 192–201. https://doi.org/10.1016/j.memsci.2010.06.032

Barrett, E.P., Joyner, L.G., Halenda, P.P., 1951. The determination of pore volume and area distributions in porous substances. I. Computations from nitrogen isotherms. J. Am. Chem. Soc. 73 (1), 373–380. https://doi.org/10.1021/ja01145a126

Bartlett, M., Bird, M.R., Howell, J.A., 1995. An experimental study for the development of a qualitative membrane cleaning model. J. Membr. Sci. 105 (1), 147–157. https://doi.org/10.1016/0376-7388(95)00052-E

Bhushan, S., Etzel, M.R., 2009. Charged ultrafiltration membranes increase the selectivity of whey protein separations [https://doi.org/10.1111/j.1750-3841.2009.01095.x]. J. Food Sci. 74 (3), E131–E139. https://doi.org/10.1111/j.1750-3841.2009.01095.x

Bird, M.R., Bartlett, M., 2002. Measuring and modelling flux recovery during the chemical cleaning of MF membranes for the processing of whey protein concentrate. J. Food Eng. 53 (2), 143–152. https://doi.org/10.1016/S0260-8774(01)00151-0

Butt, S., Hasan, S.M.F., Hassan, M.M., Alkharfy, K.M., Neau, S.H., 2019. Directly compressed rosuvastatin calcium tablets that offer hydrotropic and micellar solubilization for improved dissolution rate and extent of drug release. Saudi Pharm. J. 27 (5), 619–628. https://doi.org/10.1016/j.jsps.2019.03.002

Chen, J.P., Kim, S.L., Ting, Y.P., 2003. Optimization of membrane physical and chemical cleaning by a statistically designed approach. In.

Cordoba, N., Fernandez-Alduenda, M., Moreno, F.L., Ruiz, Y., 2020. Coffee extraction: a review of parameters and their influence on the physicochemical characteristics and flavour of coffee brews. Trends Food Sci. Technol. 96, 45–60. https://doi.org/10.1016/j.tifs.2019.12.004

Dizge, N., Soydemir, G., Karagunduz, A., Keskinler, B., 2011. Influence of type and pore size of membranes on cross flow microfiltration of biological suspension. J. Membr. Sci. 366 (1), 278–285. https://doi.org/10.1016/j.memsci.2010.10.010

Flores-Valdez, M., Meza-Márquez, O.G., Osorio-Revilla, G., Gallardo-Velázquez, T., 2020. Identification and quantification of adulterants in coffee (Coffea arabica L.) using FT-MIR spectroscopy coupled with chemometrics. Foods 9 (7). https://doi.org/10.3390/foods9070851

Gadelmawla, E.S., Koura, M.M., Maksoud, T.M.A., Elewa, I.M., Soliman, H.H., 2002. Roughness parameters. J. Mater. Process. Technol. 123 (1), 133–145. https://doi.org/10.1016/S0924-0136(02)00060-2

Groen, J.C., Peffer, L.A.A., Pérez-Ramírez, J., 2003. Pore size determination in modified micro- and mesoporous materials. Pitfalls and limitations in gas adsorption data analysis. Microporous Mesoporous Mater. 60 (1), 1–17. https://doi.org/10.1016/S1387-1811(03)00339-1

Harkins, W.D., Jura, G., 1944. Surfaces of solids. XIII. A vapor adsorption method for the determination of the area of a solid without the assumption of a molecular area, and the areas occupied by nitrogen and other molecules on the surface of a solid. J. Am. Chem. Soc. 66 (8), 1366–1373. https://doi.org/10.1021/ja01236a048

Institution, B.S. (1996). Determination of the Specific Area of Powders-Part 1: BET Method of Gas Adsorption for Solids (Including Porous Materials).

Kallioinen, M., Sainio, T., Lahti, J., Pihlajamäki, A., Koivikko, H., Mattila, J., Mänttäri, M., 2016. Effect of extended exposure to alkaline cleaning chemicals on performance of polyamide (PA) nanofiltration membranes. Sep. Purif. Technol. 158, 115–123. https://doi.org/10.1016/j.seppur.2015.12.015

Kluge, S., Kose, T., Tutuş, M., 2022. Tuning the morphology and gas separation properties of polysulfone membranes. Membranes 12 (7).

Krivan, V., Barth, P., Morales, A.F., 1993. Multielement analysis of green coffee and its possible use for the determination of origin. Microchim. Acta 110 (4), 217–236. https://doi.org/10.1007/BF01245106

Lai, W., Yang, S., Jiang, Y., Zhao, F., Li, Z., Zaman, B., Fayaz, M., Li, X., Chen, Y., 2020. Artefact peaks of pore size distributions caused by unclosed sorption isotherm and tensile strength effect. Adsorption 26 (4), 633–644. https://doi.org/10.1007/s10450-020-00228-1

Leam, J.J., Bilad, M.R., Wibisono, Y., Hakim Wirzal, M.D., Ahmed, I., 2020. Chapter 7 - membrane technology for microalgae harvesting. In: Yousuf, A. (Ed.), Microalgae Cultivation for Biofuels Production. Academic Press, pp. 97–110. https://doi.org/10.1016/B978-0-12-817536-1.00007-2

Li, H., Chen, V., 2010. Chapter 10 - membrane fouling and cleaning in food and bioprocessing. In: Cui, Z.F., Muralidhara, H.S. (Eds.), Membrane Technology. Butterworth-Heinemann, pp. 213–254. https://doi.org/10.1016/B978-1-85617-632-3.00010-0

Li, Q., Elimelech, M., 2004. Organic fouling and chemical cleaning of nanofiltration membranes: measurements and mechanisms. Environ. Sci. Technol. 38 (17), 4683–4693. https://doi.org/10.1021/es0354162

Liu, L., Luo, X.-B., Ding, L., Luo, S.-L., 2019. 4 - Application of nanotechnology in the removal of heavy metal from water. In: Luo, X., Deng, F. (Eds.), Nanomaterials for the Removal of Pollutants and Resource Reutilization. Elsevier, pp. 83–147. https://doi.org/10.1016/B978-0-12-814837-2.00004-4

Luis, P., 2018. 1.5.2 Temperature polarization. Fundamental Modeling of Membrane Systems - Membrane and Process Performance. Elsevier,. ⟨https://app.knovel.com/hotlink/pdf/id:kt011PTJ82/fundamental-modeling/temperature-polarization⟩.

Majeed, T., Phuntsho, S., Chekli, L., Lee, S.-H., Kim, K., Shon, H.K., 2016. Role of various physical and chemical techniques for hollow fibre forward osmosis membrane cleaning. Desalin.

Water Treat. 57 (17), 7742–7752. https://doi.org/10.1080/19443994.2015.1080631

Manios, T.K., Mattia, D., Bird, M.R., 2022. Fouling of polyethersulphone ultrafiltration membranes during the decaffeination of ground coffee brews. Food Bioprod. Process. 136, 14–23. https://doi.org/10.1016/j.fbp.2022.09.005

Manios, T.K., Mattia, D., Bird, M.R., 2023. The influence of multiple fouling and cleaning cycles upon the performance of polyethersulphone membrane filters during coffee extract decaffeination. Food Bioprod. Process. 140, 1–15. https://doi.org/10.1016/j.fbp.2023.04.007

Martín, M.J., Pablos, F. d, González, A., 1998. Characterization of green coffee varieties according to their metal content. Anal. Chim. Acta 358, 177–183.

Matthias, T., Katsumi, K., Alexander, V.N., James, P.O., Francisco, R.-R., Jean, R., Kenneth, S.W.S., 2015. Physisorption of gases, with special reference to the evaluation of surface area and pore size distribution (IUPAC Technical Report). Pure Appl. Chem. 87 (9–10), 1051–1069. https://doi.org/10.1515/pac-2014-1117

Muñoz-Aguado, M.J., Wiley, D.E., Fane, A.G., 1996. Enzymatic and detergent cleaning of a polysulfone ultrafiltration membrane fouled with BSA and whey. J. Membr. Sci. 117 (1), 175–187. https://doi.org/10.1016/0376-7388(96)00066-X

Pal, P., 2015. Chapter 5 - arsenic removal by membrane distillation. In: Pal, P. (Ed.), Groundwater Arsenic Remediation. Butterworth-Heinemann, pp. 179–270. https://doi.org/10.1016/B978-0-12-801281-9.00005-9

Peeters, J.M.M., Mulder, M.H.V., Strathmann, H., 1999. Streaming potential measurements as a characterization method for nanofiltration membranes. Colloids Surf. A: Physicochem. Eng. Asp. 150 (1), 247–259. https://doi.org/10.1016/S0927-7757(98)00828-0

Persson, K.M., Gekas, V., Trägårdh, G., 1995. Study of membrane compaction and its influence on ultrafiltration water permeability. J. Membr. Sci. 100 (2), 155–162. https://doi.org/10.1016/0376-7388(94)00263-X

Reis, M.H.M., Madrona, G.S., Ferreira, F.B., de Santana Magalhães, F., Bindes, M.M.M., Cardoso, V.L., 2019. 6 - Membrane filtration processes for the treatment of nonalcoholic beverages. In: Grumezescu, A.M., Holban, A.M. (Eds.), Engineering Tools in the Beverage Industry. Woodhead Publishing, pp. 175–207. https://doi.org/10.1016/B978-0-12-815258-4.00006-8

Sanaei, P., Cummings, L.J., 2017. Flow and fouling in membrane filters: effects of membrane morphology. J. Fluid Mech. 818, 744–771. https://doi.org/10.1017/jfm.2017.102

Susanto, H., Ulbricht, M., 2009. Characteristics, performance and stability of polyethersulfone ultrafiltration membranes prepared by phase separation method using different macromolecular additives. J. Membr. Sci. 327 (1), 125–135. https://doi.org/10.1016/j.memsci.2008.11.025

Virtanen, T., Rudolph, G., Lopatina, A., Al-Rudainy, B., Schagerlöf, H., Puro, L., Kallioinen, M., Lipnizki, F., 2020. Analysis of membrane fouling by Brunauer-Emmett-Teller nitrogen adsorption/desorption technique. Sci. Rep. 10 (1), 3427. https://doi.org/10.1038/s41598-020-59994-1

Weis, A., Bird, M.R., Nyström, M., 2003. The chemical cleaning of polymeric UF membranes fouled with spent sulphite liquor over multiple operational cycles. J. Membr. Sci. 216 (1), 67–79. https://doi.org/10.1016/S0376-7388(03)00047-4

Weis, A., Bird, M.R., Nyström, M., Wright, C., 2005. The influence of morphology, hydrophobicity and charge upon the long-term performance of ultrafiltration membranes fouled with spent sulphite liquor. Desalination 175 (1), 73–85. https://doi.org/10.1016/j.desal.2004.09.024

Wu, D.A.N., Bird, M.R., 2007. The fouling and cleaning of ultrafiltration membranes during the filtration of model tea component solutions [https://doi.org/10.1111/j.1745-4530.2007.00115.x]. J. Food Process Eng. 30 (3), 293–323. https://doi.org/10.1111/j.1745-4530.2007.00115.x

Zaidi, J.H., Fatima, I., Arif, M., Qureshi, I.H., 2005. Determination of trace elements in coffee beans and instant coffee of various origins by INAA. J. Radioanal. Nucl. Chem. 267 (1), 109–112. https://doi.org/10.1007/s10967-006-0015-y

Zhang, C., Wang, C., Liu, F., He, Y., 2016. Mid-infrared spectroscopy for coffee variety identification: comparison of pattern recognition methods. J. Spectrosc. 2016, 1–7. https://doi.org/10.1155/2016/7927286